Q-Space Analysis Applied to Polydisperse, Dense Random Aggregates

J. A. Hubbard, S. J. Eckels*, C. M. Sorensen**

(Received: 6 July 2007; accepted: 3 January 2008)

DOI: 10.1002/ppsc.200700014

Abstract

Polydisperse powders of spherical shell particles and nonspherical, three dimensionally dense aggregates were dispersed as turbulent jets through an abrupt orifice nozzle and in-situ small angle light scattering measurements were made. In contrast to traditional studies, the light scattering data were plotted versus the scattering wave vector rather than the scattering angle; we call this q-space analysis. For dense aggregates distinct power law trends emerged, similar to those discovered previously for spherical Mie scatterers. Moreover, when the system was very polydisperse, either with a broad bimodal or monotonic with extreme range, the q-space analysis provided particle size distribution information about these aerosol systems which was unapparent when plotted as a function of the scattering angle.

Keywords: light scattering, particle sizing, polydisperse particulate systems

1 Introduction

Light scattering as a function of scattering angle is an excellent tool for the unobtrusive, in-situ observation of particle size and morphology of aerosol and colloidal systems. However, the solution to Maxwell's equations for the scattering of electromagnetic radiation is difficult even for the most generalized case of spherical particles, commonly referred to as Mie theory. The solution becomes even more difficult, if not intractable, when irregularly shaped particles are considered. These computational difficulties propagate into experimental difficulties for interpretation of light scattering measurements. Recently we discovered patterns in the Mie scattering phase function for homogeneous spheres, scattered intensity versus scattering angle, that give simplicity to analysis [1–4]. If the scattered intensity is plotted versus the scattering wave vector q instead of the scattering angle θ, power law trends readily appear that are not seen versus θ. Our previous work showed that these trends lent simplicity to the visualization of the phase function. The purpose of this work is to show with experiment that these trends appear in light scattering data for spherical shells and nonspherical, irregularly shaped, three dimensional (nonfractal) particles. We then use this to detect extreme cases of polydispersity, which are not detectable when the phase function is plotted versus θ. These results indicate the usefulness of the q-space power laws that could provide a foundation for a new quantitative analysis in the future.

2 Background

We have shown that when the Mie scattering phase function is plotted versus the scattering wave vector q, where

$$q = 4\pi\lambda^{-1}\sin(\theta/2), \tag{1}$$

and where λ is the wavelength of the incident light and θ is the scattering angle, the patterns shown schematically

* J. A. Hubbard, Prof. S. J. Eckels, Department of Mechanical and Nuclear Engineering, 3002 Rathbone Hall, Kansas State University, Manhattan, KS 66506 (USA).

** Prof. C. M. Sorensen (corresponding author), Physics Department, 116 Cardwell Hall, Manhattan, KS 66505, 785-532-1626 (USA).
E-mail: sor@phys.ksu.edu

© 2008 WILEY-VCH Verlag GmbH & Co. KGaA, Weinheim

in Figure 1 emerge [1,4]. Figure 1 shows the envelopes of the phase function which ignore the finer ripple structure. In experiment this ripple structure is washed out for fairly mild polydispersity of geometric width 1.22 or greater [4]. The overall trends in the remaining envel-

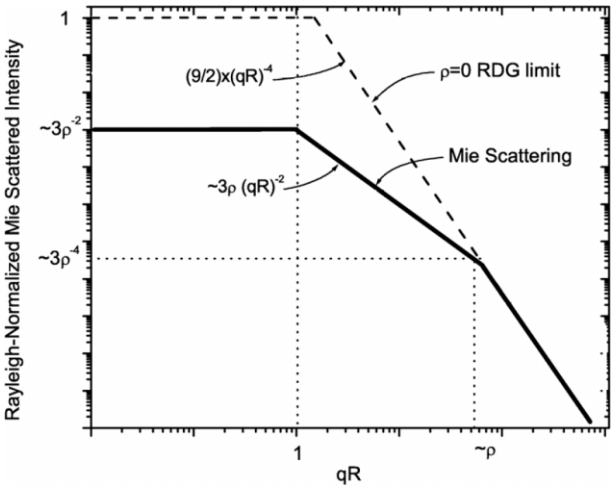

Fig. 1: q-space patterns in light scattering from spherical particles of radius R and phase shift parameterρ. In this example $\rho \simeq 55$ for the thick line. The intensity has been normalized by the Rayleigh scattering that would occur from the particles if the Rayleigh calculation was applicable.

opes show power laws of q^0 (i.e. constant) for small q which crosses over through a Guinier regime near $qR_g = 1$ to q^{-2} for intermediate q. Here R_g is the radius of gyration equal to $\sqrt{3/5}\,R$ for a sphere of radius R. Particle size measurements can be made in the Guinier regime via the Guinier equation [3],

$$I(q) = I(0)\left(1 + q^2 R_g^2/3\right)^{-1}. \quad (2)$$

Usually application of the Guinier equation is limited to a regime for which $qR_g < 1$. We have found, however, that this equation works for the entire q^0 to q^2 regime. We shall use this fact below.

Finally, near $q = \rho R_g^{-1}$, where ρ denotes the phase shift parameter, the envelopes cross over to $I \propto q^{-4}$ for large q. The phase shift parameter is given by

$$\rho = 4\,\pi\,R\,\lambda^{-1}(m-1) \quad (3)$$

where m is the refractive index of the particle. The envelopes are parameterized by the phase shift parameter, that is, all phase function envelopes lie on nearly the same curve for the same ρ, regardless of R and m. Subsequent work has shown that these trends extend into the geometric limit [5] and persist with multiple scattering [6].

3 Experimental Methods

Light scattering measurements were preformed on a variety of powders that were aerosolized by a homemade device. About 10 grams of powder were placed in a cylindrical chamber of volume 400 cc prior to each experiment. Compressed air was then injected down through a stainless steel tube directly at the powder bed. Throughout the experiment a gear motor and propeller were operated at 250 rpm to mechanically agitate the powder in the chamber. This constant stirring and air flow helped create aerosols of constant concentration. After entrainment, the particles exited the mixing chamber through a 3/32″ (2.38 mm) diameter abrupt orifice nozzle as a turbulent jet. This caused significant shear which aided in breaking apart agglomerates of particles. In-situ light scattering measurements were then made 2.5 cm from the nozzle outlet in the aerosol jet.

Our small angle light scattering device was modeled after the design by Ferri [7]. A laser beam with $\lambda = 488$ nm, polarized in the vertical direction, was used as the source of incident light. The scattered intensity was collected in the horizontal plane via a lens. The Fourier plane of this first lens was imaged by a second lens onto a linear photodiode array. The photodiode array provided intensity measurements for scattering angles in the range of 0.5° to 10°, corresponding to a q range of 1000 cm^{-1} to 23,000 cm^{-1}. This range for q implies we can measure particles from 0.4 μm to 10 μm (inverse q) with this device.

4 Results

4.1 Spherical Glass Shells

The hollow glass spheres were dispersed through the aerosol generator with a few different pressures and small angle light scattering measurements were made. The manufacturer described these particles with a nominal radius of 4–6 μm and with a bimodal size distribution shown as solid circles in Figure 2. Our analysis of the size data gave a geometric mean radius of R = 1.2 μm and geometric standard deviation of $\sigma = 2.7$.

The scattering results are shown in Figure 3. All scattered intensity data in this figure, and the rest of this work, are normalized to unity at small q. Without normalization, the data would be shifted due to changes in the absolute concentration. This would make relative comparisons between the data more difficult. No differences in light scattering data are observed as a function of flow pressure. This implies that the spheres were completely dispersed at the lowest pressure. Also notice the

© 2008 WILEY-VCH Verlag GmbH & Co. KGaA, Weinheim

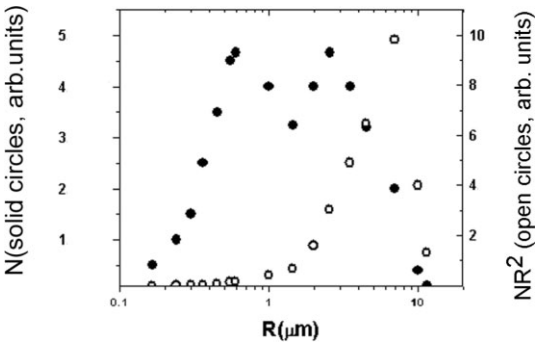

Fig. 2: Number based size distribution data for hollow glass spheres. Solid circles: Size distribution for hollow glass spheres. Open circles: Size distribution weighted by R^2.

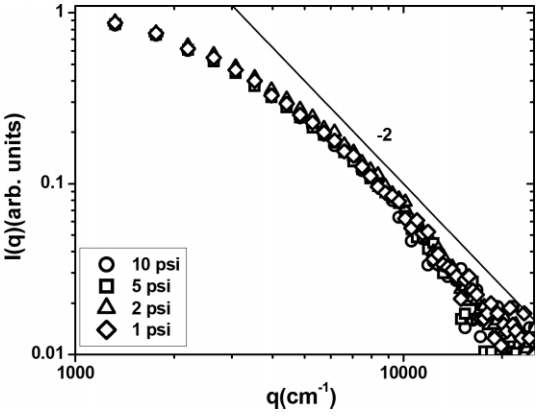

Fig. 3: Scattered intensity versus scattering wave vector for hollow glass spheres dispersed with various pressures.

absence of characteristic Mie ripples. This is attributed to the polydispersity of the system.

Trends similar to those in Figure 1 are observed in the data. At small q the slope approaches 0 and transitions to –2 as q increases. The q^{-4} regime is not observed in this data, or any other data to be described below. We infer that for the hollow glass spheres this is because the crossover at $q = \rho/R$ is out of the range of the detector at large q. To check this, consider the light scattering weighted mean size is 6.25 μm (see below). The refractive index of the glass is 1.5. To account for the hollowness of the spheres we find the effective $(m-1)$ as equal to the volume fraction of glass in the hollow sphere times the glass value of $(m-1) = 0.5$. The spheres have a density of 1.1g/cc, whereas the density of glass is 2.6 g/cc, hence we find the effective $(m-1) = 0.21$. This leads to $\rho = 34$ (assuming $R = \sqrt{5/3}R_g$) and implies the q^{-4} regime should begin when $q > 5 \cdot 10^4\,\mathrm{cm}^{-1}$, which is beyond our q range. We conclude that spherical shells display the same q^0 and q^{-2} regimes as do homogeneous spherical particles.

The data follow the same trends exhibited by Mie scatterers even though the aerosol is polydisperse, and in actuality, very few systems of interest are truly monodisperse. It has been shown that a set of particles with a geometric standard deviation of 1.22 follows the patterns of Figure 1 [4]. Our data show that systems with even larger degrees of polydispersity, e.g., geometric standard deviation of 2.7, also follow these trends. This is not surprising. This means that small angle light scattering cannot distinguish this "modest" degree of polydispersity. Certainly it can be argued that the size distribution displayed in Figure 2 is rather broad and not modest. However, as we will show below, this polydispersity is modest compared to much more broadly distributed systems which show their effect in our analysis. Thus, we designate the term "modest polydispersity" to describe any aerosol that does not destroy the single particle trends of Figure 1.

The data of Figure 3 were fit with the Guinier equation Eq. (2) in the Guinier regime to obtain an average radius of gyration of 6.25 μm. This measured radius of gyration is much larger than the geometric mean of the number based size data provided by the manufacturer. This discrepancy can be explained by the fact that light scattering measures the mean weighted by the light scattering per particle which is greater for large particles. For example, in the forward scattering regime, for particles with small phase shift parameters, the weighting factor is R^6. For these particles with $\rho = 34$ the weighting is approximately R^2. Figure 2 also shows the number distribution multiplied by R^2 (shown as open circles) and one can see the peak is now near 6 μm, consistent with the light scattering.

4.2 Dense Random Aggregates

The next system we describe is commercially available NanoActive™ MgO. Aggregates of NanoActive™ MgO are shown in Figure 4. These aggregates are describable as dense, random aggregates. By "dense" we mean non-fractal, having mass that scales with the cube of their linear dimension, hence a dimensionality of three. They are aggregates of smaller solid primary particles apparently randomly put together; hence their shape is non-spheroidal and their surfaces are rough. The primary particles are platelets roughly 400–500 nm across and 10 nm thick. A mean aggregate diameter of 3.3 μm is provided by the manufacturer.

Small angle light scattering data for dispersal with a variety of pressures are shown in Figure 5. An evolution in the data is observed as the pressure increases. At low dispersal pressure (2 psi) the data appear to exhibit the Mie scattering trends of Figure 1 for homogeneous

 © 2008 WILEY-VCH Verlag GmbH & Co. KGaA, Weinheim

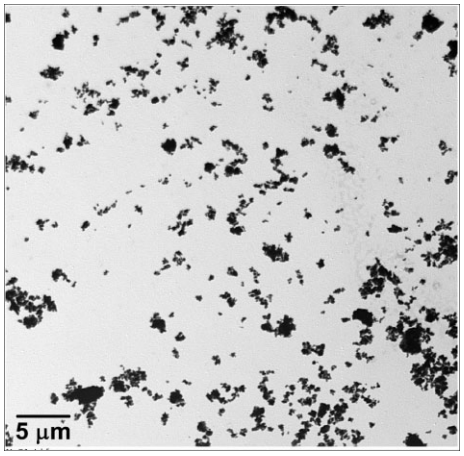

Fig. 4: TEM of NanoActive™ MgO dense random aggregates.

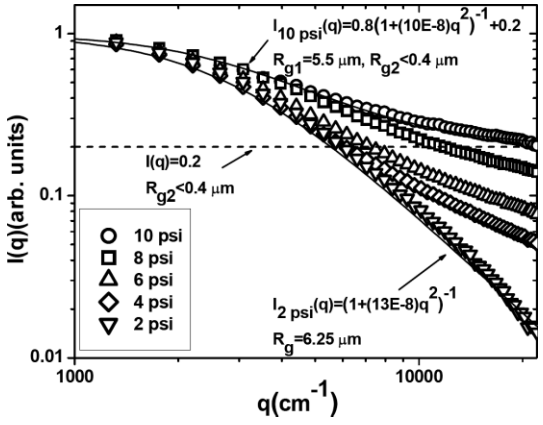

Fig. 5: Scattered intensity versus scattering wave vector for NanoActive™ MgO dense random aggregates dispersed with various pressures. The solid line(s) is the fit to the Guinier equation(s). The dashed line is the constant scattering due to particles so small that their Guinier regime is at q-values larger than that detectible by the experimental light scattering apparatus.

spheres despite being non-spherical, dense random aggregates of smaller particles. We observe the crossover from 0 to –2 slope and a significant q^{-2} regime. Hence we conclude that dense random aggregates show the same two regimes, q^0 and q^{-2}, as do spherical Mie scatters. We also conclude that this aerosol fits our definition of modest polydispersity. Guinier analysis of the data yields a mean size of $R_g = 6.25$ μm in qualitative agreement with the manufacturer size and Figure 4 accounting for light scattering weighting. The index of refraction of MgO is 1.736 hence the mean ρ value is 150 (assuming $R = \sqrt{5/3}R_g$). This implies a crossover from q^{-2} to q^{-4}, if it exists, at $q > 1.9 \cdot 10^5\,\mathrm{cm}^{-1}$. This is well above our largest accessible q, thus we do not expect the q^{-4} regime to be observed, and it is not seen in the data.

At larger dispersal pressures, the light scattering data begin to deviate from the pattern in Figure 1. The Guinier regime changes only slightly to indicate the aggregates were slightly smaller. More significant and somewhat novel is the concave upward curvature seen near $q \approx 8{,}000\ \mathrm{cm}^{-1}$ due to an increase in intensity at higher q. This signifies a dramatic increase of smaller particles which would have a Guinier regime at larger q values above our maximum q. One explanation for the substantial increase of small particles (possibly primary particles) is that the surfaces of the aggregates were being eroded during the higher pressure dispersion. This would lead to highly bimodal size distributions similar to those found in other powder processing operations such as grinding [8].

Under this assumption, the small angle light scattering data can be fitted by the superposition of two Guinier curves, one for the aggregates and another for smaller, fragmented aggregates, possibly the primary particles. The smaller mode in the bimodal distribution due to the fragmented particles was assumed smaller than the lower size limit of the detection equipment, i.e. $R_g < 0.4$ μm which corresponds to $q > 2.5 \cdot 10^3\,\mathrm{cm}^{-1}$. For this particle size the Guinier regime occurs at q greater than that detectable by our equipment. This means the scattered intensity for this mode is constant for all q in our experimental range and is shown by the dotted line in Figure 5. The large mode can be represented simply by the Guinier equation Eq. (2). By summing the Guinier curves for both modes, the experimental data were fit nicely with the aggregate size $R_g = 5.5$ μm, and the ratio of scattered intensities large to small was 4. The important point is that two modes are revealed with mean sizes that differ by at least an order of magnitude. In contrast to the definition above of modest polydispersity, we shall term this "bimodal-polydisperse".

An important observation central to the purpose of this paper is that plotting scattered intensity versus q log-log combined with the knowledge that dense three dimensional objects, whether they are spheres or compact dense aggregates, scatter with a similar identifiable pattern (Figure 1) exposed the bimodal size distribution. The same data are plotted versus the scattering angle θ and shown in Figure 6. It is apparent that something is occurring as the pressure increases, but it is more difficult to interpret than when represented as a function of q. Indeed, there is no pattern to break down when the system becomes more than modestly polydisperse since no pattern exists when plotting versus θ. Figure 6 is merely a series of indistinguishable curves.

4.3 Arizona Test Dust

The last powder dispersed in this study was fine grade Arizona test dust (ISO 12103-1 test dust). The largest

© 2008 WILEY-VCH Verlag GmbH & Co. KGaA, Weinheim

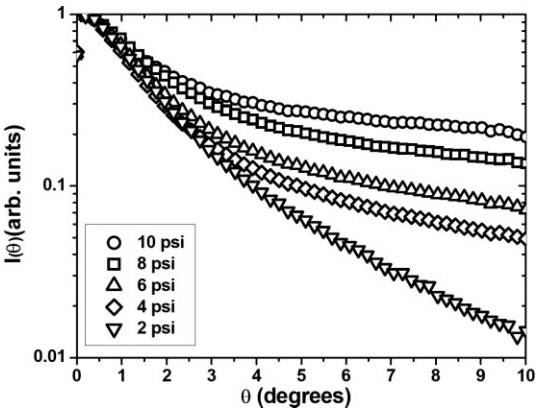

Fig. 6: Scattered intensity versus scattering angle for NanoActive™ MgO dense random aggregates dispersed with various pressure (same data as Figure 5).

components of this powder are aluminum oxide and silicon dioxide. A representative ensemble of aggregates imaged with transmission electron microscopy is shown in Figure 7.

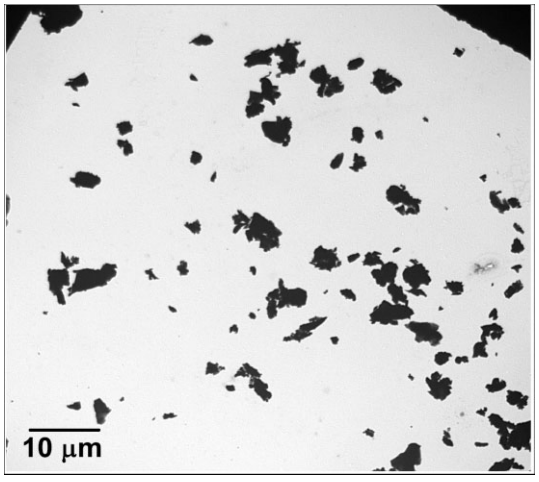

Fig. 7: TEM image of Arizona test dust aggregates.

The supplier provided data from which a cumulative size distribution based on volume (mass) was plotted [9]. The distribution is shown in Figure 8 and is seen to cover two orders of magnitude in particle size.

The powder was dispersed with increasing pressure through the aerosol generator and small angle light scattering measurements were made. The data are shown in Figure 9. The increasing presence of smaller particles with higher flow pressures is indicated by increased relative intensity at higher q. As in the experiment with NanoActive™ MgO, this can be explained by deaggregation as the powder is dispersed at higher velocities.

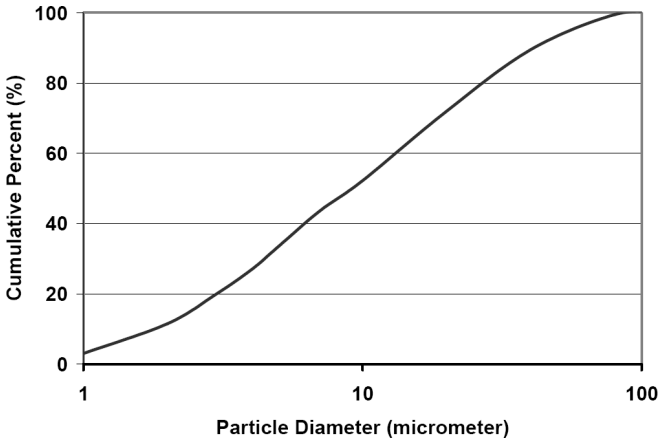

Fig. 8: Arizona Test dust volume based cumulative size distribution [9].

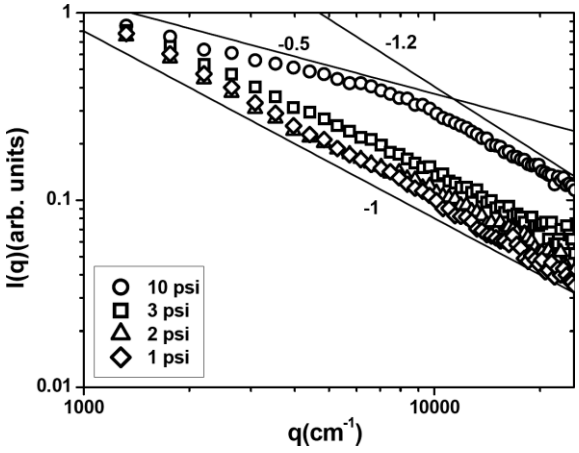

Fig. 9: Scattered intensity versus scattering wave vector for Arizona test dust dispersed with a variety of pressures.

However, a more accurate size description is difficult because of the lack of familiar trends. The characteristic Guinier regime is absent to imply the intensity weighted mean size is greater than 10 μ, consistent with Figure 8. Furthermore, slopes of –1 at lower dispersal pressures and ranging from –0.5 to –1.2 at higher pressures are observed. Nowhere do we see the –2 slope characteristic of spheres and dense, three dimensional scatterers.

Since the dust particles are three dimensionally dense, as seen in the TEM of Figure 7, and since we showed above that dense three dimensional objects have the q^{-2} functionality, we expect a region of q^{-2} functionality, which we do not observe. Thus we propose that these slopes less in magnitude than –2 are due to the extreme polydispersity of the sample, shown in Figure 8. This extreme polydispersity smeared the expected slope of –2 to lesser magnitudes as observed.

© 2008 WILEY-VCH Verlag GmbH & Co. KGaA, Weinheim

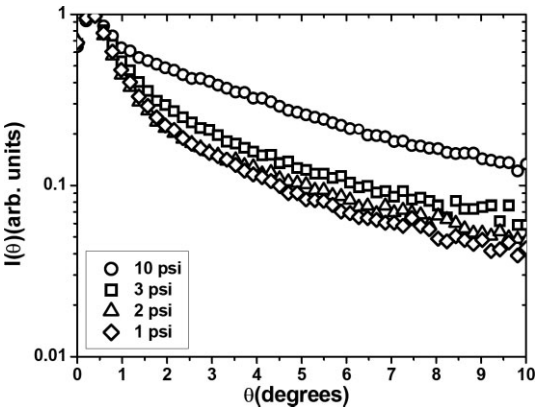

Fig. 10: Scattered intensity versus scattering angle for Arizona test dust dispersed with a variety of pressures.

The same data are plotted as a function of the scattering angle θ in Figure 10. Once again, as for the NanoActive™ MgO, the ability to characterize the aerosol as extremely polydisperse is lost in this plot because of the lack of the distinguishable trends seen when plotted in q-space.

5 Conclusions

Small angle light scattering was used to observe aerosols of spherical shell particles and non-spherical, three dimensionally dense (nonfractal) aggregates with varying degrees of polydispersity. The aerosols were dispersed through an abrupt orifice nozzle and intensity measurements were made as a function of the scattering wave vector. We found that both spherical shells and dense, three dimensional aggregates showed the same q^0 and q^{-2} power law regimes seen in Mie scattering from large phase shift parameter spheres when plotted versus q. A modest degree of polydispersity did not destroy this pattern. Plotting versus q resolved the bimodality of a system with a bimodal distribution when the modes were an order of magnitude apart in size, whereas plotting versus θ did not. Moreover, in systems with a very large degree of polydispersity the q^{-2} regime was washed out to lesser powers and this was used to discover such systems. Once again plotting versus θ does not allow for detection of such a polydispersity. Thus plotting scattered intensity versus q, rather than θ, is very useful for detecting such extreme polydispersities. We conclude that this unconventional q-space analysis provides a means of particle size and size distribution characterization that is not possible for more traditional analysis techniques because of the emergence of simple trends from Mie theory.

6 Nomenclature

σ	–	geometric standard deviation
m	–	index of refraction
I	–	intensity
ρ	–	phase shift parameter
R	μm	radius
R_g	μm	radius of gyration
θ	°	scattering angle
q	cm^{-1}	scattering wave vector
λ	nm	wavelength

7 References

[1] C. M. Sorensen, D. J. Fischbach, Patterns in Mie Scattering. *Optics Communications* **2000**, *173*,145–153.

[2] C. M. Sorensen, D. Shi, Guinier Analysis for Homogeneous Dielectric Spheres of Arbitrary Size. *Optics Communications* **2000**, *178*, 31–36.

[3] C. M. Sorensen, D. Shi, Patterns in the Ripple Structure of the Mie Scattering. *JOSA Communications* **2002**, *19*, 122–125.

[4] M. J. Berg, C. M. Sorensen, A. Chakrabarti, Patterns in Mie scattering: Evolution When Normalized by the Rayleigh Cross Section. *Applied Optics* **2005**, *44*, 7487–7493.

[5] M. Xu, R. R. Alfano, More on Patterns in Mie Scattering. *Optics Communication* **2003**, *226*, 1–5.

[6] J. C. Jonsson, G. B. Smith, G. A. Niklasson, Experimental and Monte Carlo Analysis of Isotropic Multiple Mie Scattering. *Optics Communication* **2004**, *240*, 9–17.

[7] F. Ferri, Use of a Charge Coupled Device Camera for Low-Angle Elastic Light Scattering. *Review of Scientific Instruments* **1997**, *68*, 2265–2274.

[8] R. Hogg, A. J. Dynys, H. Cho, Fine grinding of aggregated powders. *Powder Technology* **2002**, *122*, 122–128.

[9] Powder Technology Inc. **2006 May 5**. *Powder Technology Inc.* <*http://www.powdertechnologyinc.com*>.

© 2008 WILEY-VCH Verlag GmbH & Co. KGaA, Weinheim